Nature of the Josephson barrier in electron-beam-written $YBa_2Cu_3O_{7-\delta}$ junctions

B. M. Hinaus and M. S. Rzchowski
Physics Department, University of Wisconsin-Madison, Wisconsin 53706

B. A. Davidson and J. E. Nordman
Department of Electrical and Computer Engineering, University of Wisconsin-Madison, Wisconsin 53706

K. Siangchaew and M. Libera
Department of Materials Science and Engineering, Stevens Institute of Technology, Hoboken, New Jersey 07030
(Received 18 June 1997)

We analyze the temperature (T) dependence of the normal-state resistance R_n and critical current I_c in field-emission-gun electron-beam-written $YBa_2Cu_2O_{7-\delta}$ Josephson junctions from the electrode transition temperature (T_c) to 1.5 K. From a theoretical fit to $I_c(T)$ and $R_n(T)$ we find that the Josephson barrier exhibits properties of a small Fermi-surface area, dirty normal metal near its maximum metallic resistivity. Within conventional superconductor-normal-superconductor theory the barrier is 3.5 mean-free-paths long at T_c, with a normal-metal coherence length at T_c intermediate between the clean and dirty limits. [S0163-1829(97)01442-2]

Josephson transport in high-temperature superconducting (HTS) structures promises to reveal significant new physics due to the unusual nature of the order parameter in HTS materials. Phase-coherent transport in HTS structures has been used as a probe of the symmetry of the superconducting order parameter in several experiments,[1] and a non-s-wave nature of the order parameter has been theoretically predicted to lead to superconductor-normal (SN) interface effects.[2] Grain-boundary junctions in HTS materials have proved to be straightforward structures to fabricate, although strong evidence suggests that the Josephson barrier is influenced by cation disorder at the boundary leading to complex faceting networks[3] and nonuniform critical current densities,[4] as well as by a hole deficiency near the boundary due to disordered or deficient oxygen.[5] Junctions with quantifiable barrier properties are required for a detailed investigation of Josephson transport in HTS materials.

Broad-area electron irradiation of HTS materials has been demonstrated to reduce T_c as a result of oxygen displacement without cation disorder.[6,7] Several groups[8,9] have shown that HTS films in which a narrow barrier with reduced T_c has been created by *focused* electron-beam irradiation can display the Josephson effect in a limited temperature range below the electrode T_c. The absence of cation disorder in these barriers makes them excellent candidates for interpreting the Josephson effect in HTS structures if the barrier properties can be quantified. We have recently demonstrated[9] that improved techniques of nm-scale electron irradiation with a high-brightness focused electron beam allow the fabrication of $YBa_2Cu_3O_{7-\delta}$ (YBCO) Josephson barriers with T_c suppressed to zero. These barriers are narrow enough to demonstrate the Josephson effect from the 90 K critical temperature of the electrodes to below 1.5 K. In this paper we show that this wide temperature range of Josephson behavior enables the microscopic properties of the barrier to be determined from the temperature dependence of the junction critical current I_c and normal-state resistance R_n. These are extracted from fits of the current-voltage characteristics to overdamped junction theory. We show that the barrier has a decreased Fermi-surface area and a decreased mean free path relative to the unirradiated YBCO electrodes. This understanding of the nature of the barrier is essential to interpretation of effects predicted to be characteristic of HTS junctions.

Epitaxial thin films of YBCO were grown on 3 mm diameter disk-shaped $LaAlO_3$ substrates by pulsed laser deposition as described previously.[9] The samples were patterned for four-point measurements of four 2.5 μm-wide by 10 μm-long links per substrate, with twelve contact pads on the perimeter of the disk. A small slot cut in each substrate permitted *in situ* focusing and alignment of the electron beam. All unirradiated samples showed resistive transition temperatures greater than 90 K and critical current densities greater than 2×10^6 A/cm^2 at 77 K. Electron-beam irradiation was done in a Philips CM-20 scanning transmission electron microscope (STEM) equipped with a field-emission gun (FEG) electron source and a liquid-nitrogen-cooled sample stage which maintained the sample at $\sim$110 K during irradiation. Linear scribing doses ($\sim1\times10^{12}$ electrons/μm and 0.5 nA beam current) were similar to those used previously.[9] The focused electron beam has an approximate diameter of $\sim$1.5 nm under these conditions. Scribing the electron beam across the width of the link produced a continuous nm-scale line of HTS material modified by oxygen displacement. Transport measurements were done in a μ-metal-shielded liquid-helium cryostat, and magnetic fields were applied perpendicular to the sample substrate. Electrical leads to the sample were low-pass filtered at the entrance to the cryostat, and the samples were cooled in an rf-shielded room with electrical leads disconnected to minimize trapped flux.

Figure 1 shows the dynamic resistance dV/dI as a function of bias current for a typical sample at temperatures between 37 and 62.8 K. Each data set (open circles) was taken at the value of applied field that maximizes the critical current. The inset to Fig. 1, illustrating the magnetic-field dependence of the critical current for temperatures of 51.2,

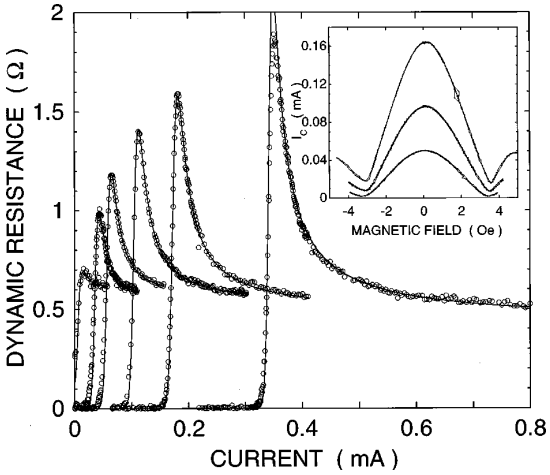

FIG. 1. Dynamic resistance dV/dI vs bias current for temperatures of 62.8, 54, 51.2, 47.1, 43.3, and 37 K. The open circles are experimental data and the solid lines a fit the Ambegaokar-Halperin overdamped junction theory, indicating RSJ behavior. The inset shows the magnetic-field dependence of the critical current for 51.2, 47.1, and 43.3 K.

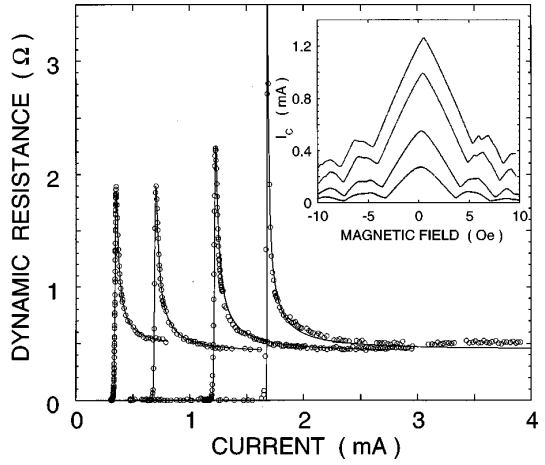

FIG. 2. Dynamic resistance dV/dI vs bias current for temperatures of 38.1, 29, 21.7, and 16.1 K. The solid lines are fits to AH theory phenomenologically extended to include excess current. The inset shows the magnetic-field dependence of the critical current for 38.8, 31.6, 23.9, and 19.9 K.

47.1, and 43.3 K, shows that this field is often very close to zero but increases slightly as the temperature is lowered due to self-fields and slight asymmetries in the sample. The solid line is a fit to the Ambegaokar-Halperin (AH) theory[10] of finite-temperature VI characteristics in heavily overdamped Josephson junctions using a least-squares criterion. The quality of fit indicates that the junctions are well-described by conventional phenomenological theory in this temperature range, with the fit parameters containing the microscopic physics. The AH theory contains three fitting parameters: the unfluctuated critical current $I_{co}=2eE_J/\hbar$ with E_J the Josephson coupling energy,[11] the junction normal-state resistance R_n, and the noise temperature T_N. We find the noise temperature to be within 30% of the actual temperature for all measurements. Our previously reported higher noise temperatures[9] were determined prior to rf filtering of the electrical leads. This indicates that much if not all of the noise observed previously was extrinsic to the junction.

The inset to Fig. 1 shows $I_c(H)$ obtained by adjusting the current with a closed-loop feedback technique to maintain a constant dynamic resistance of $\approx R_n/2$. The nonzero minimum $I_c(H)$ illustrates the beginning of a crossover from short to long junction behavior as the temperature is lowered. These three temperatures correspond to w/λ_J of 1.8, 2.5, and 3.3, where w is the junction width perpendicular to the transport current and $\lambda_J=[\Phi_o/2\pi(2\lambda_L+d)\mu_o J_c]^{1/2}$ is the Josephson penetration depth. Here J_c is determined from uniform current flow and the maximum $I_c(H)$.

Figure 2 shows dV/dI data for the temperature range below 40 K. Here the dynamic resistance is too sharply peaked to fit the AH theory well, although we find that a phenomenological fit including excess current accurately describes the data. R_n and I_{co} are then still well-defined. The data indicate weak coupling even at the lowest temperature, showing no indications of a crossover to the ''flux-flow'' behavior characteristic of a strongly coupled link.[12] Such resistively shunted junction-like behavior down to low temperature is expected from a superconductor-normal-superconductor (SNS) junction even in the wide ($w/\lambda_J \gtrsim 4$) limit.[13] The inset shows $I_c(H)$ obtained as in the inset to Fig. 1. Data for temperatures (w/λ_J) of 38.8 K (4.3), 31.6 K (6.1), 23.9 K (8.1), and 19.9 K (9.1) are shown. The predominantly linear field dependence of the low-field critical current at low temperature indicates long junction behavior, consistent with estimates of w/λ_J.

Figure 3 shows $I_{co}R_n$ extracted as fit parameters discussed above. The inset shows a semilogarithmic plot of the same data. Each experimental data point, shown in Fig. 3 as filled circles, corresponds to a dynamic resistance curve obtained at the (small) applied magnetic field that maximizes the critical current. As shown below, the initial exponential increase of the measured $I_{co}R_n$ with temperature and the saturation at low temperature is consistent with conventional theory of SNS junctions. The dashed lines through the data points are derived from the de Gennes form[14] of the high-temperature

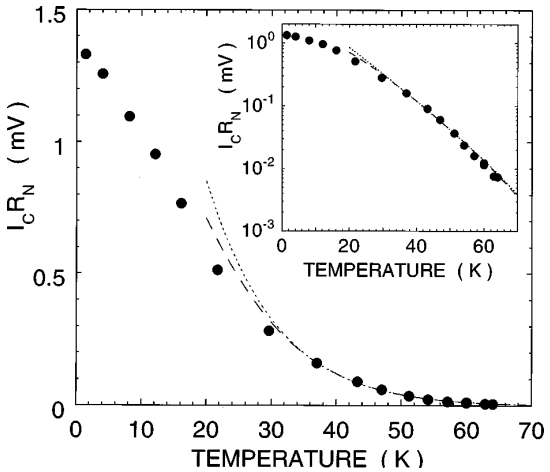

FIG. 3. Temperature dependence of $I_{co}R_n$ extracted from fits as in Fig. 1. The open circles are experimental data, and the dashed (dotted) line is a fit of the high-temperature data to the de Gennes theory of SNS proximity effect in the clean (dirty) limit. The inset shows the same data on a logarithmic scale.

limit of such conventional theory, and are seen to fit the data in the narrow-junction ($w/\lambda_j \lesssim 4$) range.

Although the possible d-wave nature of the HTS electrodes may influence some aspects of this interpretation, we argue from the consistency of our results that low-T_c proximity-effect theory at the level invoked here correctly describes the characteristic lengths of the problem. The characteristic length for Cooper pair transport in the barrier is the normal-metal coherence length (Ref. 15) ξ_n. The ratio of this length to the barrier mean free path l determines whether transport occurs in the clean $\xi_n/l \ll 1$ (ballistic transport, $\xi_{nc}/l = \hbar\tau^{-1}/2\pi kT$) or dirty $\xi_n/l \gg 1$ [diffusive transport, $\xi_{nd}/l = (\hbar\tau^{-1}/6\pi kT)^{1/2}$] limit. Here τ^{-1} is the barrier scattering rate. The critical current of the junction is a strictly decreasing function of L/ξ_N, where L is the barrier length in the transport current direction. de Gennes[14] derived an approximate form in the dirty limit

$$I_{co}R_n \approx \left(\frac{\pi\Delta}{2e}\right)\left(\frac{\Delta}{kT_c}\right)[L/\xi_n(T)]\exp[-L/\xi_n(T)], \quad (1)$$

where Δ is the temperature-dependent energy gap of the electrodes. This is shown in Fig. 3 with the T dependence of ξ_n determined from the clean (dashed line) and dirty (dotted line) limit expressions. The dirty-limit fit used a temperature-dependent mean free path proportional to $R_n^{-1}(T)$. The weak temperature dependence of Δ in the fitting range makes its exact form unimportant: we use a BCS form. This two-parameter fit to the narrow-junction temperature range of the data gives the ratio $L/\xi_N(T_c)$ and the gap ratio $\Delta(0)/kT_c$. For the sample of Fig. 3 we find $L/\xi_N\ (T_c) = 10.2$ and $\Delta(0)/kT_c = 0.5$ for the clean-limit fit, and $L/\xi_N\ (T_c) = 10.8$ and $\Delta(0)/kT_c = 0.7$ for the dirty-limit fit. Although the de Gennes form is strictly valid only in the dirty limit, such agreement in fit parameters indicates an insensitivity to the exact temperature dependence of ξ_n. As shown later, a direct evaluation of $\xi_N(T_c)/l$ from the experimental data indicates that at T_c our samples are intermediate between the clean and dirty limits. For the eight samples discussed here, we find in the dirty-limit values of $L/\xi_N\ (T_c)$ between 9 and 12 and $\Delta(0)/kT_c$ varying from 0.3 to 0.8.

Figure 4 shows the low-current ($I = 1\ \mu$A, $J \approx 8\times10^2$ A/cm^2) resistive transition (V/I) (solid line) and the normal-state resistance (filled circles) extracted from fits to the VI curves. The measured resistance above the normal state of the electrodes is $\sim 100\ \Omega$. The plateau below 85 K represents the temperature range in which the electrodes are superconducting, but the Josephson coupling energy, $E_J = \hbar I_{co}/2e$, is much less than kT. Here thermal fluctuations disrupt Cooper pair transport. Below ~ 60 K, $E_J > kT$ and supercurrent transport causes the measured low-current V/I to drop rapidly. The open circles are the normal-state barrier resistance from AH fits to the VI characteristics (Figs. 1 and 2). They continue the linear decrease shown by the resistive transition (solid line) until starting to increase below 25 K.

Because the ratio ξ_n/l is a function only of the scattering rate τ^{-1} in both the clean and dirty limit [see discussion preceding Eq. (1)], it can be determined from the temperature-dependent normal-state resistance of Fig. 4. A resistivity linear in temperature has been parametrized in HTS materials as a T-linear reciprocal mean free path or

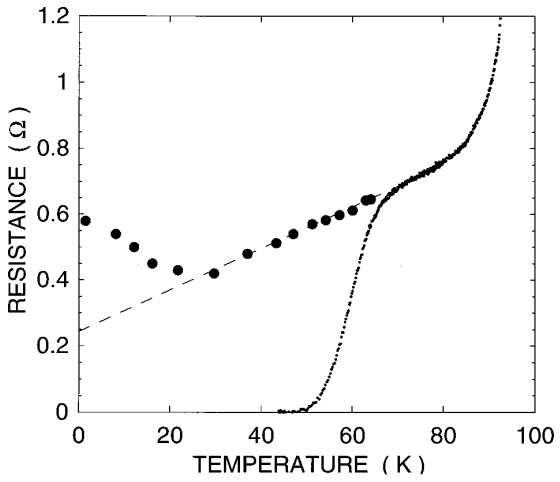

FIG. 4. Resistive transition (1 μA excitation, dots) and R_n extracted from the fits of Fig. 1 (solid circles) as a function of temperature.

scattering rate for quasiparticles.[16] Within Boltzmann transport the resistivity can then be written as[17]

$$\rho(T) = \frac{16\pi^2 R_Q}{S_F}\,(\overline{l_{\rm imp}^{-1}} + \alpha T) \approx \frac{16\pi^2 R_Q}{S_F\,\overline{\nu_F}}\,(\overline{\tau}_{\rm imp}^{-1} + \gamma T), \quad (2)$$

where we have assumed zero conductivity in the c direction. In the first formula S_F is the surface area of the Fermi surface, $R_Q = h/4e^2 \approx 6.5\ \mathrm{k}\Omega$ is the resistance quantum, $l_{\rm imp}$ is the impurity mean free path averaged over the Fermi surface, and α is a constant. In the second formula, $\overline{\nu_F}$ and $\overline{\tau_{\rm imp}}$ are the Fermi velocity and impurity scattering time averaged over the Fermi surface. $\gamma = 2\pi k\lambda_{tr}/\hbar$ in an electron-phonon interpretation of the T-linear term, with λ_{tr} a dimensionless constant.[18] Our analysis here does not rely on a particular interpretation of the T-linear scattering rate.

The parameters α^o and γ^o can be determined from the resistivity slope of optimally doped YBCO and an estimate of S_F^o. We approximate the YBCO Fermi surface[19] as a roughly cylindrical composite centered at $\pi\pi$ of height $4\pi/c$ (two planes/cell) and a radius determined by the doping. Using 0.16 holes/Cu away from half-filling as optimal doping, $S_F \approx 400\ \mathrm{nm}^{-2}$ in this approximation. Using $\partial\rho^o/\partial T \sim 0.85\ \mu\Omega$ cm/K for optimally doped unirradiated YBCO we find $\alpha^{-1} \sim 250$ nm K. A typical Fermi velocity of 10^7 cm/s then results in $\lambda_{tr} \sim 0.4$, in agreement with other estimates.[18] Based on large-area irradiation studies,[7] we assume $\lambda_{tr} \approx \lambda_{tr}^o$. We show later that S_F is strongly influenced by e-beam irradiation through a changing carrier concentration as predicted by recent theoretical calculations.[20] This irradiation-dependent S_F can be eliminated in a ratio of slope to intercept of $\rho(T)$ to give a characteristic temperature,

$$T_{\rm eff}^{-1} \equiv (\partial\rho_n/\partial T)/\rho_n(0) = \alpha\overline{l_{\rm imp}} \approx \gamma\,\overline{\tau_{\rm imp}}. \quad (3)$$

Here we take $\rho_n(0)$ to be the *extrapolated* intercept of the T-linear portion of $\rho(T)$. This allows a direct calculation of ξ_n/l at T_c from the experimental data as

$$\xi_{nc}/l = (1 + t_{\rm eff})\lambda_{tr}, \quad \xi_{nd}/l = [(1 + t_{\rm eff})\lambda_{tr}/2]^{1/2}. \quad (4)$$

The interpolation formula (Ref. 21) $\xi_n^{-2}=\xi_{nc}^{-2}+\xi_{nd}^{-2}$ gives a range of 0.3 to 0.5 for the samples studied and a value of ~ 0.31 for the sample shown in Figs. 1–4. This indicates that ξ_n (90 K)$/l$ is intermediate between the clean and dirty limits. This conclusion is consistent with the similar fit parameters and quality of fit for the clean- and dirty-limit fits to $I_{co}(T)$ shown in Fig. 3.

The product of L/ξ_n (T_c) and ξ_n $(T_c)/l(T_c)$, extracted from the $I_{co}(T)$ and $R_n(T)$ data, respectively, gives $L/l(T_c)$, showing that the barrier is approximately 3.5 mean-free-paths long at T_c for the sample of Figs. 1–4, and between 3 and 6 for the 8 samples discussed here. From Eq. (3) $L/l=(R_n/R_Q)(S_FA/16\pi^2)$, where $A=1.25\times 10^5$ nm^2 is the cross-sectional area of the barrier. Equating these results at T_c gives

$$\frac{S_F}{S_F^o}=\frac{L}{l(T_c)}\,\frac{1}{R_n(T_c)A}\,\frac{\partial\rho^o/\partial T}{\alpha^o}, \tag{5}$$

where the first two ratios are determined experimentally from the data and the last from unirradiated YBCO. A typical Fermi velocity of 10^7 cm/s gives $S_F/S_F^o\approx 0.13$. Optimal doping corresponds to slightly less than half-filling where the Fermi surface is large, centered around $\pi\pi$, and increasing slowly in surface area with increasing hole doping.[22] Reducing the hole concentration moves the system toward half-filling. Experimental results[23] suggest that S_F shrinks substantially during this process, possibly resulting in pockets around $\pi/2,\pi/2$.

Using Eqs. (2) and (3) we find

$$l(T_c)/l^o(T_c)=(1+t_{\rm eff})^{-1}(\overline{\nu_F}/\overline{\nu_F^o}) \tag{6}$$

using the approximate zero resistance intercept of unirradiated YBCO. Substitution of the experimental values gives $0.6\overline{\nu_F}/\overline{\nu_F^o}$ for the ratio. This indicates that disorder has been introduced into the barrier region, most probably oxygen defects given our beam energy of 200 keV. Since we expect a decreased ν_F corresponding to the reduced S_F, Eqs. (5) and (6) indicate at least a 12 times reduction in $S_Fl(T_c)$. Equation (2) then gives $\rho(T_c)\geqslant 1.2$ mΩ cm, leading to an effective barrier length, $L\leqslant 9$ nm. This reflects both a reduced hole doping and a reduced mean free path. It is consistent with the upturn in resistance at low temperature in Fig. 4 in indicating an approach to the maximum metallic resistivity. Assuming a cylindrical Fermi surface, we find $k_Fl\approx 3.5$ at the resistance minimum, comparable with previous estimates.[24]

We have shown that FEG/STEM-written YBCO Josephson junctions demonstrate quantifiable overdamped SNS behavior over a wide temperature range below T_c. This enables characterization of the barrier through theoretical fits of the IV characteristics. Estimates of the most important barrier ratios (ξ_n/l, L/l, and S_F/S_F^o) depend only on λ_{tr}, established to be unchanged by irradiation. This barrier characterization in a HTS junction displaying well-understood SNS behavior over a broad temperature range promises to elucidate the unique features of HTS Josephson transport.

This research was supported by NSF Grant No. DMR-92-1407.

[1] For a review see, D. J. Van Harlingen, Rev. Mod. Phys. **67**, 515 (1995).
[2] C. R. Hu, Phys. Rev. Lett. **72**, 1526 (1994); J. H. Xu, J. H. Miller, and C. S. Ting, Phys. Rev. B **53**, 3604 (1996); H. X. Tang, Z. D. Wang, and J. X. Zhu, *ibid.* **54**, 12 509 (1996).
[3] I. F. Tsu, S. E. Babcock, and D. K. Kaiser, J. Mater. Res. **11**, 1383 (1996).
[4] M. Daumling, E. Sarnelli, P. Chaudhari, A. Gupta, and J. Lacey, Appl. Phys. Lett. **61**, 1355 (1992); O. M. Froehlich, H. Schulze, A. Beck, B. Mayer, L. Alff, R. Gross, and R. P. Huebner, *ibid.* **66**, 2289 (1995).
[5] V. P. Dravid, H. Zhang, and Y. Y. Wang, Physica C **213**, 353 (1993).
[6] A. Legris, J. Phys. I (France) **3**, 1605 (1993); S. N. Basu, T. E. Mitchell, and M. Nastasi, J. Appl. Phys. **69**, 3167 (1991).
[7] S. K. Tolpygo *et al.*, Phys. Rev. B **53**, 12 462 (1996).
[8] S. K. Tolpygo *et al.*, Appl. Phys. Lett. **63**, 1696 (1993); A. J. Pauza *et al.*, Physica B **194-196**, 119 (1994).
[9] B. A. Davidson, J. E. Nordman, B. M. Hinaus, M. S. Rzchowski, K. Siangchaew, and M. Libera, Appl. Phys. Lett. **68**, 3811 (1996).
[10] V. Ambegaokar and B. I. Halperin, Phys. Rev. Lett. **22**, 1364 (1969).
[11] M. Tinkham, *Introduction to Superconductivity*, 2nd ed. (McGraw-Hill, New York, 1996).
[12] N. F. Heinig *et al.*, Appl. Phys. Lett. **69**, 577 (1996).
[13] D. Berman, HSJ van der Zant, T. P. Orlando, and K. Delin, IEEE Trans. Appl. Supercond. **3**, 2273 (1993).
[14] P. G. de Gennes, Rev. Mod. Phys. **36**, 225 (1964).
[15] K. K. Likharev, Rev. Mod. Phys. **51**, 101 (1979).
[16] A. Carrington *et al.*, Phys. Rev. Lett. **69**, 2855 (1992).
[17] N. F. Mott, *Conduction in Non-Crystalline Materials* (Clarendon, Oxford, 1987).
[18] M. Gurvitch and A. T. Fiory, Phys. Rev. Lett. **59**, 1337 (1987).
[19] Rong Liu, B. W. Veal, A. P. Paulikas, J. W. Downey, P. J. Kostic, S. Fleshler, U. Welp, C. G. Olson, X. Wu, A. J. Arko, and J. J. Joyce, Phys. Rev. B **46**, 11 056 (1992).
[20] Raju P. Gupta and Michele Gupta, Phys. Rev. Lett. **77**, 3216 (1996).
[21] K. A. Delin and A. W. Kleinsasser, Supercond. Sci. Technol. **9**, 227 (1996).
[22] O. K. Anderson *et al.*, Phys. Rev. B **49**, 4145 (1994); W. E. Pickett *et al.*, Science **255**, 46 (1992).
[23] D. S. Marshall *et al.*, Phys. Rev. Lett. **73**, 4841 (1996).
[24] G. S. Boebinger *et al.*, Phys. Rev. Lett. **77**, 5417 (1996).